Control Systems for Induction Machines with Magnetic Saturation

Charles R. Sullivan, *Student Member, IEEE,* Chaofu Kao, Brian M. Acker, and Seth R. Sanders, *Member, IEEE*

***Abstract*— Extensions of field-oriented control methods for induction machines, accounting for magnetic saturation, are developed. The new methods are based on a nonlinear π model for the saturated machine. This model is a more accurate representation of the saturation phenomena in the machine than are most previous models, and it is shown to also facilitate development of control algorithms. Observers for estimating rotor flux are also discussed. Experimental results verifying operation of one proposed control method are presented.**

I. Introduction

INDUCTION machines are usually modeled with the assumption of linear magnetics. However, in many variable-torque applications, it is desirable to operate in saturation, allowing an induction machine to produce higher torque. For example, in vehicular applications, the induction machine may be sized for normal road conditions. However, to overcome extreme inclines or to permit high acceleration and deceleration rates, it is necessary to produce high instantaneous torque. Thus, a smaller machine may be used if its control system can maintain control through peak torque demand. Traditionally, inductance values used for control or calculations are adjusted to compensate for saturation effects. However, this is not always adequate. More precise modeling of saturation becomes essential for control purposes and for understanding the limitations imposed by saturation. This paper develops a new model for saturation and discusses its implications for control systems.

It has been recently noted that saturation effects in smooth air-gap machines can introduce cross-coupling effects that are not predicted by linear models. In a two-axis machine (or model) the current in one winding can affect the flux in the orthogonal winding. The "cross saturation" model [1]–[8] has become the standard method of accounting for these effects. The model is based on the conventional T model of an induction motor, and the saturation is assumed to be entirely in the mutual inductance, not in the leakage. While the T model with saturating mutual inductance gives reasonable accuracy in simulations, it can be inconvenient to use when the machine is connected to a voltage source, since it is most naturally a current-controlled rather than a flux-controlled model. In [4], for example, the T model is transformed to a π model for the purposes of simulation.

Manuscript received March 15, 1994; revised June 13, 1995. This work was supported by an NSF graduate fellowship, a GE graduate fellowship, and an NSF Young Investigator award.

The authors are with the Department of Electrical Engineering and Computer Sciences University of California, Berkeley, CA 94720–1772 USA.

Publisher Item Identifier S 0278-0046(96)01269-5.

Because the form of the T model with saturating mutual inductance is merely postulated by extending a standard linear model to include saturation of the mutual path, our work develops a new model, based on a nonlinear magnetic circuit model of the machine [9], [10]. The resulting machine model is in fact most naturally a π model, and so we avoid the need to transform it for simulations and/or control designs. Although the π model can provide a more accurate model for the saturated induction machine, of greater importance, the π form is more convenient for field-oriented control designs that take magnetic saturation into account.

Field-oriented control decouples the control of rotor flux and torque in the linear-magnetics case. However, cross-saturation effects can severely disrupt performance of a control system designed without taking these effects into account [11]. Although control systems based on the T model and the use of a current source inverter have been developed to mitigate these problems [6], [12]–[14], the resulting designs are somewhat awkward. In contrast, with the flux-controlled π model, by using the stator flux as an intermediate control variable, it is possible to obtain a simple decoupled control of rotor flux and torque. Our approach relies on the use of a fast control loop around a voltage source inverter to control stator flux. Stator flux is then used as an intermediate control variable, as is stator current in current-fed control schemes.

As with standard field-oriented control, a method of estimating rotor flux without direct measurement is desirable, and we discuss several methods for doing this with the new model. Measurements taken on a 3-hp wound rotor induction machine show good correlation with our model. We refer the reader to [9] for details. The present paper includes a description of an experimental set-up of the proposed control system, along with detailed test results.

II. Magnetic Circuit Modeling

To model a saturating magnetic structure we use conventional magnetic circuit modeling, augmented by the use of nonlinear reluctances to represent sections of saturable steel or other soft ferromagnetic material. The B-H characteristic of the steel is assumed to be a single-valued nonlinear monotonic function. The flux/MMF characteristic of the reluctance element, for simple geometries, is just the B-H characteristic, scaled by cross-sectional area for flux, and by length for MMF.

Fig. 1(a) shows a simplified tooth structure for a single pair of teeth in an induction machine. Fig. 1(b) shows one way of drawing a magnetic circuit model for the tooth pair, making

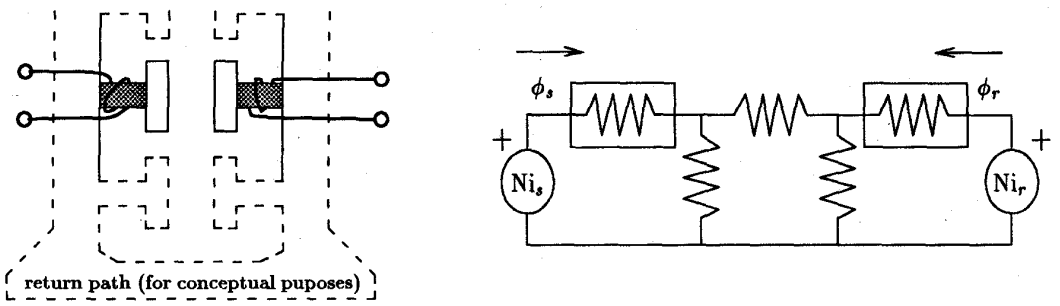

(a) (b)

Fig. 1. Model of tooth pair. (a) Simplified physical structure. (b) Corresponding magnetic circuit. Boxed elements are nonlinear.

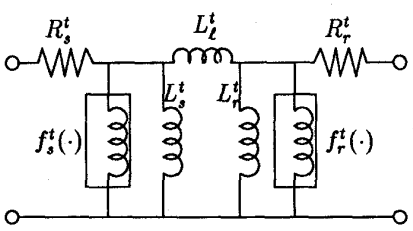

Fig. 2. Electric circuit of tooth pair.

the assumption that the only portions of the steel that saturate are the central legs, shown shaded in Fig. 1(a).

Through a series of transformations [9], the magnetic circuit can be shown to be equivalent to the electric circuit in Fig. 2. We separate the stator and rotor inductances into linear parts, L_s^t and L_r^t, and nonlinear parts, with flux-current relationships $f_s^t(\cdot)$ and $f_r^t(\cdot)$. The superscript t is used to indicate an inductance or function describing only a single tooth. As drawn, the circuit in Fig. 2 could have circulating currents in various loops of inductors. In the linear case these are unobservable, uncontrollable modes. In the nonlinear case, the circulating current would not appear directly at the rotor and stator terminals, yet could affect the apparent nonlinear characteristics of the inductances. There are, however, additional constraints resulting from the magnetic circuit that preclude this possibility. Namely, the flux linkage in L_ℓ^t must be equal to the difference in flux linkages in L_r^t and L_s^t, the flux linkages in $f_s^t(\cdot)$ and L_s^t must be equal, and the flux linkages in $f_r^t(\cdot)$ and L_r^t must be equal. This is reflected in the equations derived from Fig. 2.

To move from the model of a single tooth pair to a model of a symmetric induction machine, we assume a smooth air-gap and perfectly sinusoidally distributed windings. To model this structure, we consider the rotor and stator to be constructed of an infinite number of infinitesimal teeth of the type modeled above, each with the appropriate number of turns of each phase, according to the sinusoidal distribution.

The circuit model of the complete machine has the same structure as the model in Fig. 2, but each element has vector voltages and currents. We use a two-axis model, and note that the standard transformations may be used to model a three-phase machine. The nonlinear inductors are described by vector functions of the form $\vec{\imath} = F(\vec{\lambda})$. The vector direction of $\vec{\imath}$ is the same as the direction of $\vec{\lambda}$, and rotational symmetry implies that $\| \vec{\imath} \|$ depends only on $\| \vec{\lambda} \|$. As a result of these two constraints, $F(\cdot)$ may be written as

$$F(\vec{\lambda}) = f(\| \vec{\lambda} \|)\frac{\vec{\lambda}}{\| \vec{\lambda} \|}. \tag{1}$$

The function $f(\cdot)$ is a scalar function that is shaped similarly to the saturation characteristic of the individual teeth, $f^t(\cdot)$, but is produced by the combination of the saturation characteristics of the steel in many teeth acting simultaneously [9]. It may be assumed to be monotonic, and, if hysteresis is neglected, to be single valued and to pass through the origin. Note that one could consider the quantity $\| \vec{\lambda} \|/f(\| \vec{\lambda} \|)$ to be an inductance that varies as a function of $\| \vec{\lambda} \|$, so that $\vec{\imath} = \vec{\lambda}/L(\| \vec{\lambda} \|)$. This is the notation used in most discussions of the nonlinear T model, and is mathematically equivalent. We choose to use the $F(\cdot)$ notation instead, because it clarifies which terms in an equation are linear and which are not. We also choose $F(\cdot)$ to include only the nonlinear portion of the inductance, and absorb any linear part in a parallel linear inductance. With this notation, the linear-magnetics case can be obtained from any of our expressions simply by dropping the nonlinear terms.

The electrical dynamics of the system using the functions $F_s(\cdot)$ and $F_r(\cdot)$, and with rotation of the rotor are

$$\vec{\imath}_s^s = F_s(\vec{\lambda}_s^s) + \left(\frac{1}{L_s} + \frac{1}{L_\ell}\right)\vec{\lambda}_s^s - \frac{1}{L_\ell}e^{\mathbf{J}\theta}\vec{\lambda}_r^r \tag{2}$$

$$\vec{\imath}_r^r = F_r(\vec{\lambda}_r^r) + \left(\frac{1}{L_r} + \frac{1}{L_\ell}\right)\vec{\lambda}_r^r - \frac{1}{L_\ell}e^{-\mathbf{J}\theta}\vec{\lambda}_s^s \tag{3}$$

and

$$\dot{\vec{\lambda}}_s^s = \vec{v}_s^s - \mathbf{R}_s\,\vec{\imath}_s^s \tag{4}$$

$$\dot{\vec{\lambda}}_r^r = \vec{v}_r^r - \mathbf{R}_r\vec{\imath}_r^r \tag{5}$$

where θ is the electrical angle of the rotor position, $\mathbf{J}$ is the rotation matrix

$$\mathbf{J} = \begin{bmatrix} 0 & -1 \\ 1 & 0 \end{bmatrix}$$

and the overdot $(\cdot)$ indicates differentiation with respect to time. Note that L_s and L_r denote the linear parts of the magnetizing inductances associated with the stator and rotor,

respectively. They are not, as in conventional T model notation, the overall inductance measured from the stator and rotor terminals. Due to the symmetry of the machine, the resistance matrices $\mathbf{R}_s$ and $\mathbf{R}_r$ are just the identity multiplied by scalar resistances. The subscript s or r on flux linkage or current (λ or i) indicates stator or rotor quantities. The superscript s indicates that the flux or current is measured in the stator, or stationary, reference frame, and the superscript r indicates coordinates fixed to the mechanical rotation of the rotor.

Experimental measurements have been conducted on a 3-hp wound-rotor machine. Both a T model with saturation in the mutual path, and the above described π model have been fit to the measured data. The π model shows a slightly better fit [9], and is much better suited to control design as discussed in Section V.

III. Blondel-Park Transformation

The characteristics of the functions $F_s(\cdot)$ and $F_r(\cdot)$ allow moving a rotation ($e^{-\mathbf{J}\theta}$) inside or outside the function. This is useful because it allows performing the Blondel-Park transformation,

$$\begin{bmatrix} \vec{\lambda}_s^x \\ \vec{\lambda}_r^x \end{bmatrix} = T(\theta,\rho)\begin{bmatrix} \vec{\lambda}_s^s \\ \vec{\lambda}_r^r \end{bmatrix} \tag{6}$$

where

$$T(\theta,\rho) = \begin{bmatrix} e^{-\mathbf{J}\rho} & 0 \\ 0 & e^{\mathbf{J}(\theta-\rho)} \end{bmatrix} \tag{7}$$

and the superscript x indicates an arbitrary reference frame, at an angle ρ from the stator reference frame. Both θ and ρ may be time varying. The electrical dynamics become

$$\begin{bmatrix} \dot{\vec{\lambda}}_s^x \\ \dot{\vec{\lambda}}_r^x \end{bmatrix} = \begin{bmatrix} -\dot{\rho}\mathbf{J}\vec{\lambda}_s^x \\ (\dot{\theta}-\dot{\rho})\mathbf{J}\vec{\lambda}_r^x \end{bmatrix} + \begin{bmatrix} \vec{v}_s^x \\ \vec{v}_r^x \end{bmatrix} - \underline{\mathbf{R}}\left\{\underline{\mathbf{C}}_0\begin{bmatrix} \vec{\lambda}_s^x \\ \vec{\lambda}_r^x \end{bmatrix} + \begin{bmatrix} F_s(\vec{\lambda}_s^x) \\ F_r(\vec{\lambda}_r^x) \end{bmatrix}\right\} \tag{8}$$

where $\underline{\mathbf{C}}_0$ is defined by

$$\underline{\mathbf{C}}_0 = \begin{bmatrix} \left(\frac{1}{L_s}+\frac{1}{L_\ell}\right)\mathbf{I} & -\frac{\mathbf{I}}{L_\ell} \\ -\frac{\mathbf{I}}{L_\ell} & \left(\frac{1}{L_r}+\frac{1}{L_\ell}\right)\mathbf{I} \end{bmatrix} \tag{9}$$

$$\begin{bmatrix} \vec{v}_s^x \\ \vec{v}_r^x \end{bmatrix} = T(\theta,\rho)\begin{bmatrix} \vec{v}_s^s \\ \vec{v}^r{}_r \end{bmatrix} \tag{10}$$

and $\underline{\mathbf{R}}$ is the 4×4 matrix of stator and rotor resistance. The principle benefit of the transformation is the removal of angular dependence from the dynamics (8), so that the system becomes time-invariant for constant speed $\dot{\theta}$. The transformation can be used to change to any reference frame, by the appropriate choice of ρ. This will be useful for field-oriented control. We use different superscripts to designate the transformed quantities in different reference frames, summarized in Table I. The field-oriented reference frame is discussed further in Section V.

TABLE I

superscript designation	reference frame	ρ
s	Stator	$\rho = 0$
r	Rotor	$\rho = \theta$
x	Arbitrary	ρ
e	Field-Oriented	$\angle(\vec{\lambda}_r^s)$

IV. Torque Production

Since many common methods of calculating torque are valid only for linear magnetics, we must carefully calculate torque for the nonlinear-magnetics case. Because our model is flux-controlled it is most straight forward to calculate the torque as a function of flux and angle by differentiating the field energy.[1]

$$\tau(\vec{\lambda}_s^s, \vec{\lambda}_r^r, \theta) = -\frac{\partial W_f(\vec{\lambda}_s^s, \vec{\lambda}_r^r, \theta)}{\partial \theta}. \tag{11}$$

We calculate W_f by $\int \vec{\imath}^T\, d\vec{\lambda}$, resulting in

$$W_f = \left[-\frac{1}{L_\ell}e^{\mathbf{J}\theta}\vec{\lambda}_r^r\right]^\top \vec{\lambda}_s^s + (\theta \text{ independent terms}). \tag{12}$$

The torque is then

$$\tau(\vec{\lambda}_s^s, \vec{\lambda}_r^r, \theta) = \left[\frac{1}{L_\ell}\mathbf{J}e^{\mathbf{J}\theta}\vec{\lambda}_r^r\right]^\top \vec{\lambda}_s^s \tag{13}$$

or in terms of the Park-transformed flux

$$\tau(\vec{\lambda}_s^x, \vec{\lambda}_r^x, \theta) = \left[\frac{1}{L_\ell}\mathbf{J}\vec{\lambda}_r^x\right]^\top \vec{\lambda}_s^x = -\frac{1}{L_\ell}(\lambda_{sd}^x\lambda_{rq}^x - \lambda_{sq}^x\lambda_{rd}^x). \tag{14}$$

This expression is identical to one form of the expression for the torque with linear magnetics. It can be shown to be equivalent to another common form

$$\tau = \vec{\imath}_s^{\,s\top}\mathbf{J}\vec{\lambda}_s^x. \tag{15}$$

V. Field-Oriented Control

In field-oriented control, the use of a reference frame oriented in the direction of the rotor flux vector results in decoupled control of rotor flux and torque [6], [15]. For use with the nonlinear flux-controlled model, we formulate the field-oriented control method in terms of flux vectors as state variables. We first discuss the control as if we had available measurements of all state variables. Later sections will discuss methods of measuring or estimating relevant variables. To transform to the rotor field-oriented reference frame, we use the Park transformation as discussed above, with ρ set equal to the angle of the rotor flux vector $\vec{\lambda}_r^s$. We use the superscript e, for electrical, to designate variables in the rotor field-oriented reference frame, since, in steady state, this reference frame rotates at the same frequency as the supply voltage. Setting

[1] We use the convention that torque is positive in the motoring direction.

$\rho = \angle(\vec{\lambda}_r^s)$ is equivalent to constraining λ_{rq}^e to be zero, and results in

$$\dot{\rho} = \frac{R_r}{L_\ell}\frac{\lambda_{sq}^e}{\lambda_{rd}^e} + \dot{\theta}. \tag{16}$$

The other electrical equations become

$$\dot{\lambda}_{rd}^e = -R_r\left[\left(\frac{1}{L_r}+\frac{1}{L_\ell}\right)\lambda_{rd}^e - \frac{1}{L_\ell}\lambda_{sd}^e + f_r(\lambda_{rd}^e)\right] \tag{17}$$

$$\dot{\vec{\lambda}}_s^e = -\dot{\rho}\mathbf{J}\vec{\lambda}_s^e + \vec{v}_s^e - R_s\left\{\left(\frac{1}{L_s}+\frac{1}{L_\ell}\right)\vec{\lambda}_s^e - \frac{1}{L_\ell}\begin{bmatrix}\lambda_{rd}^e\\0\end{bmatrix} + F_s(\vec{\lambda}_s^e)\right\} \tag{18}$$

where $f_r(\cdot)$ is the scalar version of $F_r(\cdot)$, as in (1), and the rotor voltage is zero for shorted rotor windings or shorted rotor bars. The mechanical equations become

$$\dot{\omega} = \frac{1}{J_{\text{inertia}}}\left(\frac{1}{L_\ell}\lambda_{sq}^e\lambda_{rd}^e - \tau_{\text{load}}\right) \tag{19}$$

$$\dot{\theta} = \omega. \tag{20}$$

These equations, though formulated in terms of flux, reduce to the familiar equations for field-oriented control when they are reformulated in terms of stator current, and the nonlinear terms are dropped. Unfortunately, nonlinear terms in the conversion to a stator current formulation add cross coupling, destroying the simplicity of the control. Similar cross coupling in a T model has been shown in simulations to cause significant disruptions when control algorithms that ignore it are used [11]. However, cross coupling does not appear in the flux formulation in (16)–(20) above, except in the stator flux dynamics (18). Here lies one of the advantages of the π model with respect to the T model. By viewing stator flux as a control variable, as opposed to stator current, we obtain a simple decoupled control for rotor flux magnitude and for torque. Specifically, the component of the stator flux aligned with the rotor flux can be used to control rotor flux magnitude, per (17), while the orthogonal component of stator flux can be used to control torque, per (19).

Note that the rotor flux control loop does have a nonlinearity not present in the linear-magnetics case. But this subsystem is not hard to control. It can be stabilized with simple linear feedback, or may be linearized with feedback by using

$$\lambda_{sd}^e = L_\ell\left\{\left(\frac{1}{L_r}+\frac{1}{L_\ell}\right)\lambda_{rd}^e + f_r(\lambda_{rd}^e)\right\} - K_d\frac{L_\ell}{R_r}(\lambda_{rd}^e - \tilde{\lambda}_{rd}^e) \tag{21}$$

where K_d is the desired linear feedback coefficient.

Since control of stator flux provides decoupled control of torque and rotor flux, the stator flux command is used as an input to a subsystem that controls the stator flux through the use of a voltage-source inverter. The design of this subsystem controlling the stator dynamics

$$\dot{\vec{\lambda}}_s^e = -\dot{\rho}\mathbf{J}\vec{\lambda}_s^e + \vec{v}_s^e - R_s\left\{\left(\frac{1}{L_s}+\frac{1}{L_\ell}\right)\vec{\lambda}_s^e - \frac{1}{L_\ell}\begin{bmatrix}\lambda_{rd}^e\\0\end{bmatrix} + F_s(\vec{\lambda}_s^e)\right\} \tag{22}$$

is very similar to the design of such a controller for the linear-magnetics case, as discussed in [6], [15], [16]. The controller subtracts the terms for resistive drop and speed voltage in (22), so that the system looks simply like an integrator. The rest of the control can then be as simple as linear feedback

$$\tilde{\vec{v}}_s^e = K_s(\tilde{\vec{\lambda}}_s^e - \vec{\lambda}_s^e) + \cdot\rho\mathbf{J}\vec{\lambda}_s^e + R_s\left\{\left(\frac{1}{L_s}+\frac{1}{L_\ell}\right)\vec{\lambda}_s^e - \frac{1}{L_\ell}\begin{bmatrix}\lambda_{rd}^e\\0\end{bmatrix} + F_s(\vec{\lambda}_s^e)\right\} \tag{23}$$

where $\tilde{}$ indicates a commanded value.

The only difference that saturation makes in the design of this inner stator flux-control loop is the addition of $F_s(\cdot)$ in the term representing resistive drop in (23). If stator current is measured, the measured current may be used in the control, and so the characteristics of the nonlinearity are not needed for the controller. The control is then

$$\tilde{\vec{v}}_s^e = K_s(\tilde{\vec{\lambda}}_s^e - \vec{\lambda}_s^e) + \dot{\rho}\mathbf{J}\vec{\lambda}_s^e + R_s\vec{i}_s^e. \tag{24}$$

Thus in this implementation the control is completely independent of the magnetic saturation, except for the rotor nonlinearity's effect on the rotor flux magnitude control loop, where it may be ignored. This is in contrast to a similar system, based on the nonlinear T model in [13]. The system in [13] is shown to require additional terms to cancel cross coupling due to the nonlinearity. Although the control based on the π model is independent of the magnetic nonlinearity, this is not true of the observers, so a complete implementation will require knowledge of the nonlinearity.

A. Other Methods

In the linear-magnetics case, cross coupling in the stator dynamics can be removed simply by using a current-source inverter. However, if the equations for the nonlinear π model (16)–(20) are directly reformulated in terms of current, the nonlinear terms add cross coupling. It is still possible to use the nonlinear π model with a current source inverter, but it requires a slightly different approach.

The control hardware or software determines the appropriate values of λ_{sd}^e and λ_{sq}^e to independently control the rotor flux and torque, respectively, just as with a voltage-source inverter. From those commands an appropriate current command is calculated, to produce that flux. Although this calculation involves cross coupling, it is straightforward because no dynamics are involved. From the equivalent of (2)

$$\tilde{\vec{i}}_s^e = F_s(\tilde{\vec{\lambda}}_s^e) + \left(\frac{1}{L_s}+\frac{1}{L_\ell}\right)\tilde{\vec{\lambda}}_s^e - \frac{1}{L_\ell}\begin{bmatrix}\lambda_{rd}^e\\0\end{bmatrix}. \tag{25}$$

Since the stator saturation characteristic introduces cross coupling, whereas the rotor saturation characteristic does not, one could consider designing a motor with a relatively small cross section of steel in the rotor, and a larger cross section in the stator. The motor could then be operated with the rotor steel moderately saturated, but with the stator steel remaining linear. This would eliminate the cross coupling, and calculation of the current commands (25) would be simplified.

VI. Flux Observers

For field-oriented control in the rotor flux reference frame, accurate estimation of the rotor flux vector is essential. Two approaches for rotor flux estimation are analyzed below.

A. Stator-Flux-Based Observer

Since the stator voltages and currents of a squirrel cage motor can be measured directly, a stator-based observer is attractive. Some stator-based observers, such as those discussed in [17], integrate the derivative of rotor flux, calculated from measurements of stator quantities. With the nonlinear model, nonlinear dynamics in the observer and in the observer error system would result. To avoid this, we integrate stator flux instead, and then make an instantaneous calculation, involving no dynamics, of the rotor flux. The stator flux observer is defined by

$$\dot{\hat{\vec{\lambda}}}_s^s = \vec{v}_s^s - R_s \vec{i}_s^s - K_0 \hat{\vec{\lambda}}_s^s \tag{26}$$

where $\hat{}$ indicates an estimate. A decay term such as $K_0 \hat{\vec{\lambda}}_s^s$ must be used in order to make the observer asymptotically stable. The calculation of the rotor flux is accomplished by

$$\hat{\vec{\lambda}}_r^s = L_\ell \left[\left(\frac{1}{L_s} + \frac{1}{L_\ell} \right) \hat{\vec{\lambda}}_s^s + F_s(\hat{\vec{\lambda}}_s^s) - \vec{i}_s^s \right]. \tag{27}$$

Note that no speed or position estimates are required for this observer, or for the field-oriented control itself. In many systems the generation of a torque command may require these measurements, but the torque control does not. Another advantage of this observer is that the rotor saturation characteristic does not appear in the equations, and so does not need to be known. Since it is not critical to know the rotor saturation characteristic for the control either, this feature of this observer makes possible a complete control system that does not require knowledge of the rotor saturation characteristic.

Since resistance of windings and rotor bars tends to vary strongly with temperature, it is important to evaluate the sensitivity of the observer to these variations. Fig. 3(a) shows results of a numerical solution for the steady-state error in the angle of the rotor flux estimate as a function of the error in the estimate of stator resistance. Results for both the observer described here, and the same observer with the terms for magnetic saturation dropped, are shown. The greater accuracy of the observer including magnetic saturation effects is apparent. Although the observer is not very sensitive to resistance variations near full speed, it will become more sensitive at lower speeds, as the resistive drop becomes a larger portion of the stator voltage. However, unlike rotor temperature, stator temperature may be directly measured, and so the resistance calculated. Alternatively, separate coils may be used for sensing flux so that the resistive term need not be subtracted.

An important disadvantage of this observer is the necessity for the inclusion of a decay term, because the term introduces error at low frequencies. Results with linear-magnetics systems show a practical lower limit for this type of system is about 3 Hz. With separate coils used for sensing flux, systems have been reported to work well above 0.5 Hz [15]. While these results would be satisfactory for many speed-control applications, a different observer is required for position control, as discussed below.

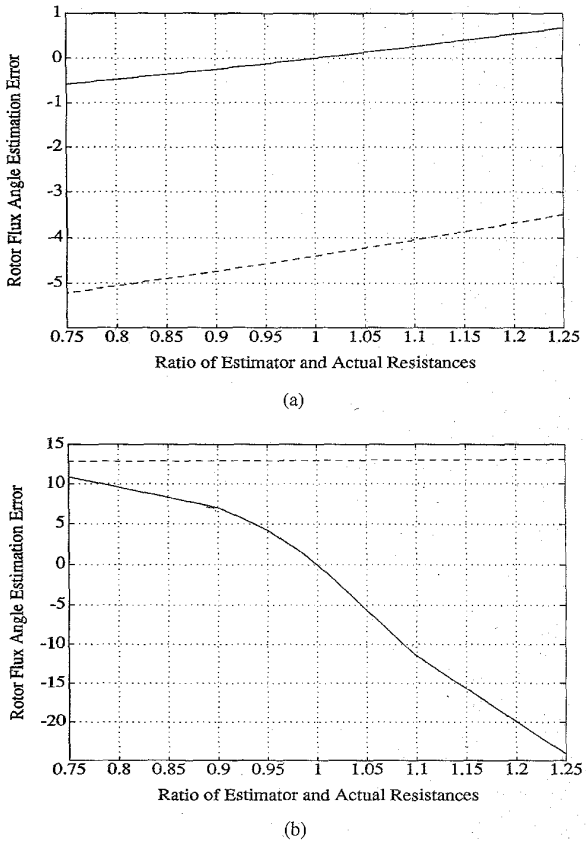

Fig. 3. Effect of resistance uncertainty on (a) stator-based observer, and (b) rotor-based observer. Steady-state error in angle (degrees) of estimated rotor flux is shown as a function of resistance error. Dotted line is observer with the nonlinear terms dropped. Numerical solution based on a supply voltage of 300 V, 60 Hz, and a slip of 10 Hz, on a 220-V, 3-hp rated machine, measured in [9].

B. Rotor-Flux-Based Observer

From (5) we construct a simulation of rotor dynamics

$$\dot{\hat{\vec{\lambda}}}_r^s = \omega \mathbf{J} \hat{\vec{\lambda}}_r^s - R_r \left[F_r(\hat{\vec{\lambda}}_r^s) + \left(\frac{1}{L_r} + \frac{1}{L_\ell} \right) \hat{\vec{\lambda}}_r^s - \frac{1}{L_\ell} \tilde{\vec{\lambda}}_s^s \right]. \tag{28}$$

The commanded value of the stator flux, $\tilde{\vec{\lambda}}_s^s$, may be used, assuming that the inverter forces the flux to quickly track the command. We use a simple open-loop simulator as an observer, and do not use correction terms as in [17], in order to avoid the additional complexity this would entail.

Because the dynamics of this observer, unlike the stator-flux-based observer, are nonlinear, it is important to look at the error dynamics to be sure that the error does always decay, and to get an estimate or bound on speed of convergence. We define $\vec{e} = \hat{\vec{\lambda}}_r^s - \vec{\lambda}_r^s$. By taking the difference between (28) and

(5), we get an equation for the error dynamics

$$\dot{\vec{e}} = \omega \mathbf{J}\vec{e} - R_r\left(\frac{1}{L_r} + \frac{1}{L_\ell}\right)\vec{e} - \frac{R_r}{L_\ell}(\tilde{\vec{\lambda}}_s^s - \vec{\lambda}_s^s) - R_r\left[F_r(\hat{\vec{\lambda}}_r^s) - F_r(\vec{\lambda}_r^s)\right]. \tag{29}$$

For stability analysis, we use the Lyapunov function

$$V(\tilde{\vec{\lambda}}_s^s, \vec{\lambda}_s^s, \hat{\vec{\lambda}}_r^s, \vec{\lambda}_r^s) = \frac{\vec{e}^\top \vec{e}}{2}. \tag{30}$$

The time derivative of this function

$$\dot{V} = \vec{e}^\top \omega \mathbf{J}\vec{e} - R_r\left(\frac{1}{L_r} + \frac{1}{L_\ell}\right)\vec{e}^\top\vec{e} - R_r\frac{1}{L_\ell}\vec{e}^\top(\tilde{\vec{\lambda}}_s^s - \vec{\lambda}_s^s) - R_r\vec{e}^\top\left[F_r(\hat{\vec{\lambda}}_r^s) - F_r(\vec{\lambda}_r^s)\right] \tag{31}$$

satisfies

$$\dot{V} \le \frac{-R_r}{L_l}\vec{e}^\top\vec{e} \tag{32}$$

provided $\tilde{\vec{\lambda}}_s^s = \vec{\lambda}_s^s$, and so the error converges at least as fast as the time constant

$$\frac{L_l}{2R_r}. \tag{33}$$

Although this observer has the advantage of being able to operate at zero speed for position control applications, it is more complex, and requires knowledge of the rotor saturation characteristic, the rotor resistance, and the speed. Fig. 3(b) shows numerical solutions for the effects of rotor resistance uncertainty on this observer, and on the same observer with the nonlinear terms neglected. Although the nonlinear observer performs better than the linear observer when the resistance error is small, it is sensitive to resistance error, and shows no advantage over the linear observer when the resistance error is very high. The sensitivity to resistance error, at this operating point, is also much greater than the sensitivity of the stator-based observer.

To further compare the performance of the stator- and rotor-based observers, the effect of leakage inductance uncertainty is simulated in Fig. 4. The two respond similarly to errors in leakage. Leakage is expected to be a much more stable parameter than resistance, since it is determined mainly by geometric factors, and so does not vary with temperature nearly as much as does resistance.

Further work may need to be done to reduce the sensitivity of the rotor-based observer to resistance error before a high-performance position control system can be designed with it. Since rotor resistance has an important effect on the performance of flux observers for the linear-magnetics case as well, there has been much work done on methods of reducing the sensitivity. These methods include adaptive identification of the resistance, and correction terms in the observer dynamics that reduce the sensitivity. These methods need to be evaluated for their ease of implementation and performance with nonlinear magnetics.

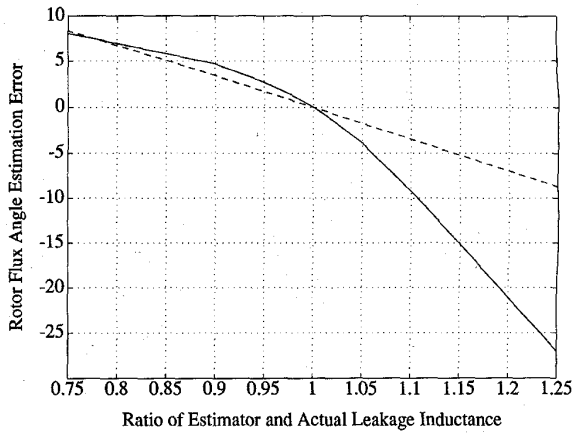

Fig. 4. Effect of leakage inductance uncertainty on observers. Error in angle (degrees) of estimated rotor flux is shown as a function of leakage inductance error. Dotted line is the nonlinear stator-based observer; solid line is the rotor-based observer.

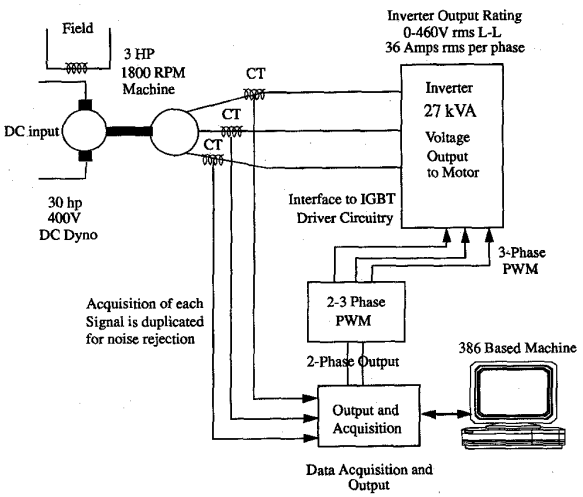

Fig. 5. Experimental setup.

VII. Experimental Setup

Our experimental setup is illustrated in Fig. 5. The induction machine used in the experiments is a 3-hp, 1800-r/min wound rotor machine, rated for 220 V rms line-to-line, and operated with the rotor shorted. It is fed from a commercial pulse-width modulated (PWM) IGBT inverter, operating at a switching frequency of 15 kHz, and rated for 36 A rms and 460 V rms line-to-line. As such, it is readily possible to drive the motor well above its ratings. A microprocessor control within the inverter was replaced with custom hardware that directly accessed the gate driver modules. The custom hardware consists of a three phase PWM modulator that interfaces with two-axis command voltages supplied by our digital controller, a 386-based personal computer.

The data collection and output to the inverter is provided by a commercial data acquisition/data output board. The data-acquisition function features an eight channel differential multiplexer, 12-bit resolution, and an overall data conversion

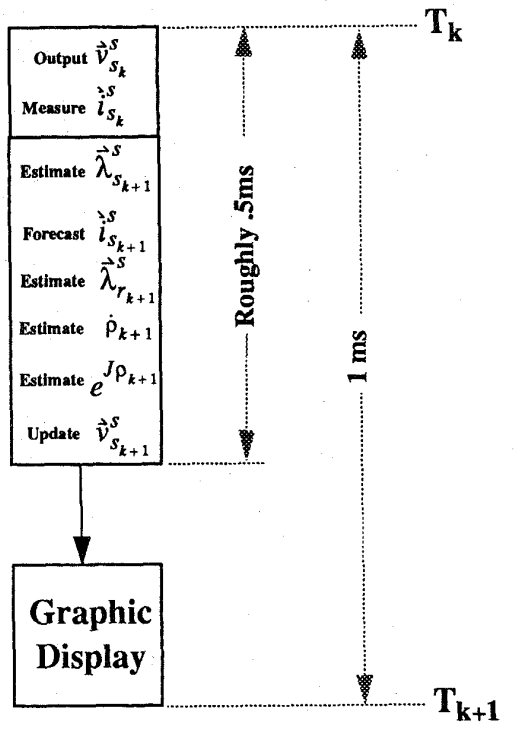

Fig. 6. Timeline for execution of control.

rate of 100 kHz. The input signals consisting of the motor phase currents are filtered prior to sampling. Since this system has excess sampling capacity, duplicate samples of each signal are obtained at each sampling time. Selection between the duplicate signal samples is accomplished by examining their proximity to estimates predicted within the control system. This greatly improves rejection of bad data that has been corrupted by noise spikes.

A 386-based personal computer is used to implement the control algorithm. Computer interrupts are generated at 1 KHz to permit a 1-ms update rate. Performance tests have shown that the control system is capable of updates at 0.5 ms. The excess time between interrupts is utilized to control the computer display. User selectable plots in the electrical reference frame and/or the stator reference frame can be displayed in real-time. Command torque and flux levels can be preprogrammed or changed in real-time from the keyboard. Both open and closed loop control and adjustments are available through keyboard interface.

A 40-kW separately excited dynamometer is used to provide adjustable loading, and is fitted with a torque scale to measure mechanical torque.

A. Implementation of Control and Flux Estimation Schemes

Our initial experimental implementation is based on the stator flux control scheme outlined in Section V coupled with the stator-flux-based rotor flux observer outlined in Section VI. Since our experimental framework restricts the update rate to be on the order of 1 ms, care needs to be taken in implementing these control and estimation schemes. For example, a delay of 1 ms at an electrical frequency of 60 Hz amounts to a phase delay of 21°, which could cause a severe disruption to any field oriented control scheme. To be precise and consistent, our algorithm is executed according to the time line shown in Fig. 6. In particular, after an interrupt at t_k, the voltage $\vec{v}^s_{s\,k}$ is fed to the inverter PWM controller through a zero-order hold. Immediately thereafter, the motor phase currents $\vec{i}^s_{s\,k}$ are sampled. Over the remainder of the 1 ms interval, the state of the flux observer is updated, the next value of the control $\vec{v}^s_{s\,k+1}$ is computed, and the computer display is updated.

A functional block diagram of the complete control algorithm is shown in Fig. 7. Conceptually, this algorithm is divided into five subblocks, which are discussed below.

Rotor Flux Estimation: This block implements a discrete time version of the stator-flux-based scheme outlined in Section VI. Specifically, during the k-th sample interval, this block uses the commanded voltage $\vec{v}_{s\,k}$, the sampled current $\vec{i}_{s\,k}$, and the stator flux estimate $\hat{\vec{\lambda}}_{s\,k}$ to update the stator flux estimate according to

$$\hat{\vec{\lambda}}_{s\,k+1} = \hat{\vec{\lambda}}_{s\,k} + T(\vec{v}_{s\,k} - R_s\vec{i}_{s\,k} - K_0\hat{\vec{\lambda}}_{s\,k}) \qquad (34)$$

where T is the (1 mS) update time and K_0 is a factor used to stabilize the observer, as previously discussed. An estimate for the rotor flux vector $\hat{\vec{\lambda}}_{r\,k+1}$ at the $(k+1)$-th sample time is then constructed using the static equation (27) from the now-available stator flux estimate and a one-step-advanced version of the measured stator current vector. The latter is developed as follows.

One-Step Prediction of Stator Current: Our control/ estimation algorithm uses a one-step-advanced version of the sampled current in some functions. To develop this predicted current vector, the sampled current vector is rotated ahead through one time step in accord with an available estimate of the electrical angular frequency. The estimate of the angular frequency is developed by numerically differentiating the estimate of the rotor flux vector with respect to time. The predicted stator current vector is constructed by

$$\hat{\vec{i}}_{s\,k+1} = e^{\mathbf{J}(\hat{\rho}_k T)}\vec{i}_{s\,k} \qquad (35)$$

with the estimate of the electrical angular velocity $\hat{\rho}_k$ developed as follows.

Estimate of Electrical Angular Velocity: Our flux estimation algorithm attempts to keep track of the instantaneous value of the rotor flux vector. As such, an estimate of the instantaneous angular position of this vector is always available. Specifically, our algorithm stores this angular information in the matrix

$$e^{\mathbf{J}\hat{\rho}_k} = \frac{1}{\|\hat{\vec{\lambda}}_{r\,k}\|}\begin{bmatrix}\hat{\lambda}_{rd\,k} & -\hat{\lambda}_{rq\,k}\\ \hat{\lambda}_{rq\,k} & \hat{\lambda}_{rd\,k}\end{bmatrix}$$

which has entries consisting of the cosine and sine of the rotor flux angle. In this way, any difficulties arising in keeping track of angle modulo 2π are avoided.

The instantaneous electrical frequency (of the rotor flux vector) is calculated by differentiating the relationship $\vec{\lambda}^e_r =$

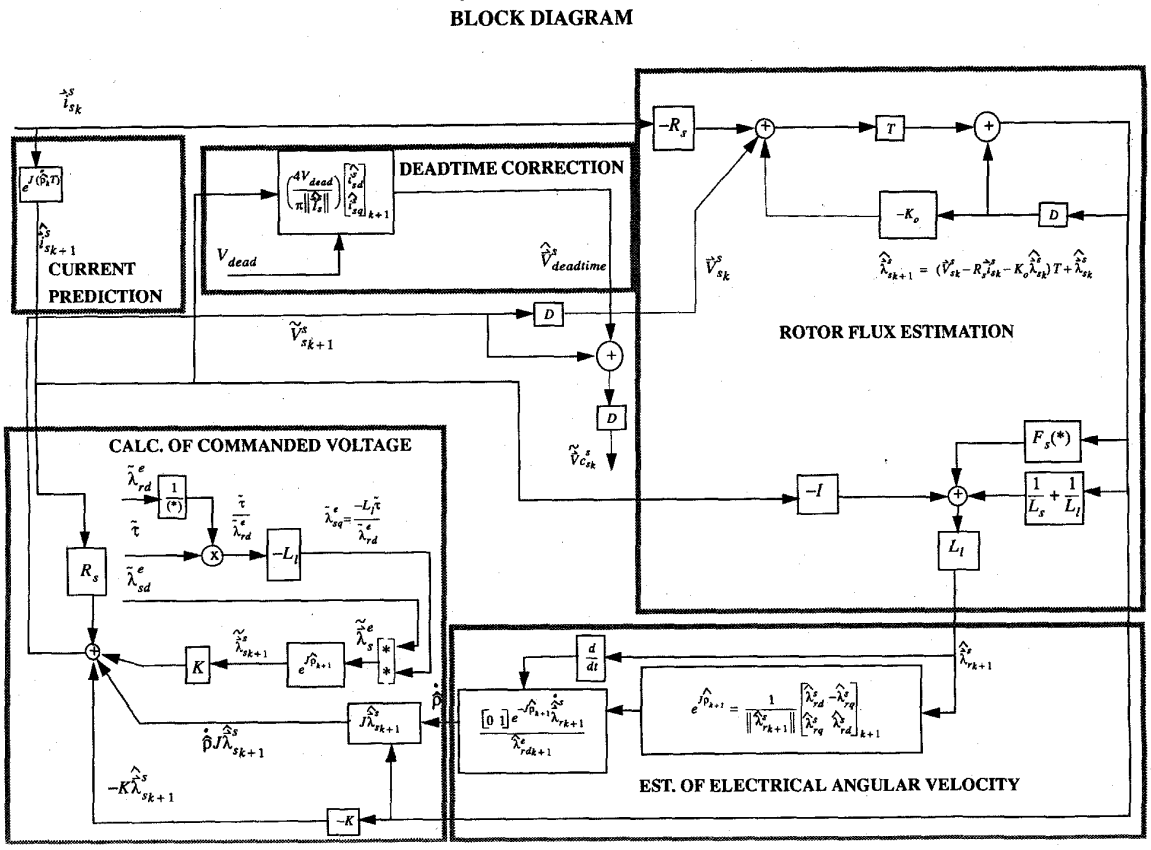

Fig. 7. Control system block diagram.

$e^{-\mathbf{J}\rho}\vec{\lambda}_r^s$, and then examining the second component of the resulting vector equation. The result is

$$\dot{\rho} = \frac{[0\ 1]e^{-\mathbf{J}\rho}\dot{\vec{\lambda}}_r^s}{\lambda_{rd}^e}. \tag{36}$$

Our algorithm develops an estimate of the electrical frequency with a band-limited numerical differentiation scheme applied to the sequence of rotor flux estimates. Note that explicit calculation and differentiation of the flux angle is always avoided.

Calculation of Command Voltage: The desired inverter voltage for step $k+1$ is calculated using the commanded torque and the commanded rotor flux magnitude, which are used to develop a commanded stator flux. In our initial experiments, the rotor flux magnitude has been controlled with an open-loop scheme where an appropriate direct axis stator flux is specified *a priori*. This corresponds to the choice $K_d = 0$ in (21).

The commanded stator flux is compared to the estimated value of this flux, $\hat{\vec{\lambda}}_{s\ k+1}$, to develop an error signal. The error signal is multiplied by a feedback gain and then added to a feedforward term comprising the predicted stator current and a predicted speed voltage. This implements the control (24).

Deadtime Correction: The final block in our algorithm is a deadtime correction scheme that attempts to counteract the voltage errors caused by deadtime in the inverter. Note that the deadtime voltage error depends only on the sign of the current in each phase of the inverter, and causes a voltage error of the form $\Delta v = -V_{\text{dead}} sgn(i)$. It turns out that attempting to directly compensate for this term is difficult since one would then need to detect the zero crossings of the current. This is difficult due to noise corrupting the current measurements, which can lead to a bouncing measured current signal. An alternative is to compensate only for the fundamental component of the deadtime voltage by multiplying the (approximately sinusoidal) current by the factor $4V_{\text{dead}}/(\pi\|\vec{i}_s\|)$ where $V_{\text{dead}} = V_{\text{DCbus}} f_s t_{\text{dead}}$ is the product of the dc bus voltage, the switching frequency, and the inverter dead time. In our system, this amounted to about 40 V. This technique is motivated by the describing function method and has been reported to be effective in [18]. In particular, this approach avoids excessive sensitivity to current zero crossings.

VIII. Experimental Results

Experiments studying instantaneous control of torque were carried out with the system described above. Specifically, our system commands a step torque waveform to allow observations of certain measured and estimated quantities. Experiments were carried out in two ways. First, we used the control law based on the nonlinear flux-current model for the magnetizing inductances in our π model. The second experiments

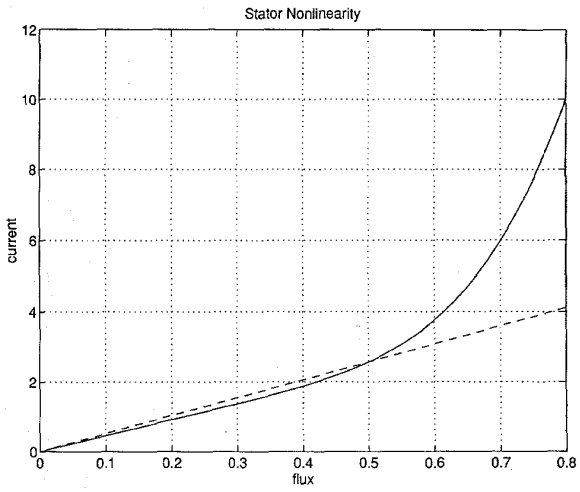

Fig. 8. Stator flux-current characteristics for saturated and linear models. Current in A and flux at V-s.

used only linear inductance models in the design of the control law. This amounted to a trivial modification where a look-up table containing the nonlinear flux-current relation for the stator is replaced with a look-up table containing a linear flux-current relation. The two flux-current curves are compared in Fig. 8. Note that the linear curve is derived from the nonlinear curve by selecting a chord corresponding to rated operation. As such, the two curves are close for flux levels below 0.5 V-s.

In all experiments, the rotor flux magnitude was programmed in an open-loop manner by simply commanding a constant level of direct axis stator flux. With this simplification, only the stator-side flux-current characteristic is needed for use in the rotor flux estimation step. In the stator-based rotor flux observer, the low frequency corner (K_0) was set at 5 rad/s. For control of the stator flux vector, our system used a bandwidth of 200 rad/s. This is conservative considering the 15-kHz switching frequency.

Step response data with the commanded rotor flux set at 0.4 and 0.6 V-s were taken. The performance of the control systems based on the linear and nonlinear models are compared in Figs. 9 and 10. Additional experimental results are resported in [19].

In Fig. 9 the performance with control systems based on the linear and nonlinear models is not very different. A useful measure of performance is the step response in torque, as calculated from the cross product of stator current and stator flux. Since stator current is directly measured, and stator flux can be estimated without using any machine parameters other than stator winding resistance, the calculation of torque from these variables is independent of the magnetics model. Both control systems give a step response in torque that follows the input command quite closely. This can be attributed to the fact that the stator is operating unsaturated. Note also that the rotor flux (fr.d) is not disturbed during the torque step.

However, the step responses with the linear and nonlinear models at the higher flux level (0.6 V-s) are drastically different. With the nonlinear flux-current model, the control system generates an essentially ideal transient response to a

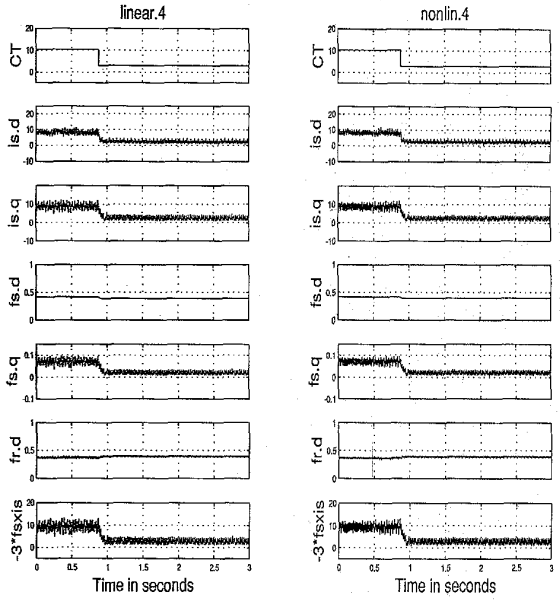

Fig. 9. Comparison of step responses for control systems based on linear and nonlinear magnetics, both with flux at 0.4 V-s. CT is the torque command in N·m. is.d and is.q are the direct and quadrature measured currents. fs.d and fs.q are the estimated stator fluxes, and fr.d the estimated rotor flux magnitude. -3*fsxis is an estimate of actual torque, from the cross product of stator current and flux.

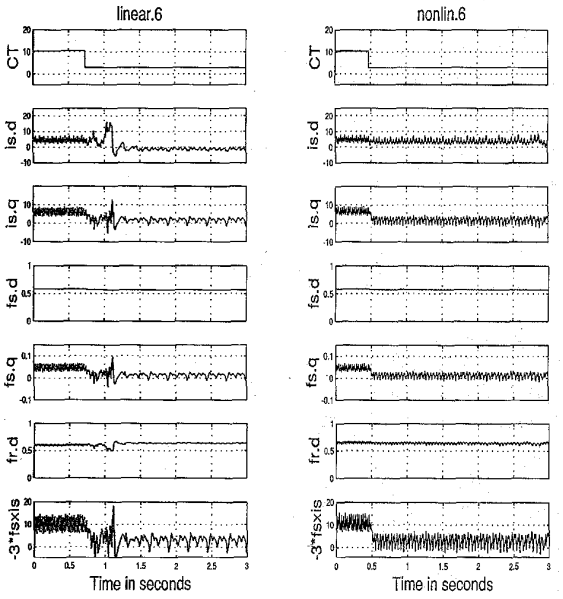

Fig. 10. Comparison of step responses comparison of step responses for control systems based on linear and nonlinear magnetics, both with flux at 0.6 V-s.

step torque command, as seen in Fig. 10. In contrast, with the standard linear flux-current model, calibrated for 0.5 V-s, the transients are far from ideal, as seen in the figure. Specifically, the estimated rotor flux and corresponding computed torque exhibit overshoot and ringing in response to the step command. Note that the rotor flux is estimated using the *linear* magnetic

model here. This disturbed transient response manifests itself with corresponding behavior on the stator terminals. Namely, the stator current also exhibits similar overshoot and ringing. This behavior corresponds to that exhibited in a detuned field-oriented control scheme, and is due to the neglect of the magnetic saturation.

IX. Conclusion

The new nonlinear π model of induction motors operating in magnetic saturation is more closely based on a physical model of the machine than is the T model. It is also more convenient to use in control design. Methods similar to standard field-oriented control can be developed relatively easily for this model. Flux observers for use with field-oriented control have also been developed. It is expected that these control systems will have superior performance than those based on the T model, both because they are based more closely on the physics of the machine, and because they can be implemented without the approximations that are necessary to derive a reasonably simple control system from the T model.

Both rotor-based and stator-based rotor flux observers have been developed. The stator-based observer is expected to be preferred for speed control applications because of its simplicity, its insensitivity to rotor resistance variations, and the fact that it does not require a speed sensor. The principle disadvantage of the rotor-based observer introduced here is its sensitivity to rotor resistance. However, it has the advantage of allowing operation to zero speed. Further work on reducing this observer's sensitivity to rotor resistance, either through adaptive estimation of the resistance, or through modification of the observer itself, may be necessary to design a high performance position control system for saturated induction machines.

An experimental implementation of a control system for a 3-hp machine using a voltage-source inverter and a stator-based rotor flux observer was implemented using a commercial inverter and a 386-based computer. The system demonstrated substantial improvements in step response when control based on linear magnetics was replaced with control based on the nonlinear π model.

References

[1] J. E. Brown, K. P. Kovacs, and P. Vas, "A method of including the effects of main flux path saturation in the generalized equations of a.c. machines," *IEEE Trans. Power Appar. Syst.*, vol. PAS-102, no. 1, pp. 96–103, Jan. 1983.

[2] P. Vas, K. E. Hallenious, and J. E. Brown, "Cross-saturation in smooth-air-gap electrical machines," *IEEE Trans. Energy Conversion*, vol. EC-1, no. 1, pp. 103–109, Mar. 1986.

[3] R. J. Kerkman, "Steady-state and transient analysis of an induction machine with saturation of the magnetizing branch," *IEEE Trans. Ind. Applicat.*, vol. IA-21, no. 1, pp. 226–234, Jan.–Feb. 1985.

[4] J. Robert, "A simplified method for the study of saturation in A-C machines," in *Modelling and Simulation of Electrical Machines and Power Systems*, J. Robert and D. K. Tran, Eds. North-Holland: Elsevier Science Publishers B. V., 1988, pp. 129–136.

[5] M. S. Garrido, L. Pierrat, and E. Dejaeger, "The matrix analysis of saturated electrical machines," in *Modelling and Simulation of Electrical Machines and Power Systems*, J. Robert and D. K. Tran, Eds. North-Holland: Elsevier Science Publishers B. V., 1988, pp. 137–144.

[6] P. Vas, *Vector Control of AC Machines*. Oxford: Oxford Univ. Press, 1990.

[7] R. D. Lorenz and D. W. Novotny, "Saturation effects in field-oriented induction machines," *IEEE Trans. Ind. Applicat.*, vol. 26, no. 2, pp. 283–9, 1990.

[8] F. M. H. Khater, R. D. Lorenz, D. W. Novotny, and K. Tang, "Saturation effects in field-oriented induction machines," *IEEE Trans. Ind. Applicat.*, vol. IA-23, no. 2, pp. 276–82, 1987.

[9] C. R. Sullivan and S. R. Sanders, "Models for induction machines with magnetic saturation of the main flux path," *IEEE Trans. Ind. Applicat.*, vol. 31, no. 4, 1995.

[10] ——, "Models for induction machines with magnetic saturation of the main flux path," in *Conf. IEEE Ind. Applicat. Soc. Annu. Meeting*, 1992, vol. 1, pp. 123–31.

[11] P. Vas and M. Alakula, "Field-oriented control of saturated induction machines," *IEEE Trans. Energy Conversion*, vol. 5, no. 1, pp. 218–223, Mar. 1990.

[12] E. Levi, S. Vukosavic, and V. Vuckovic, "Saturation compensation schemes for vector controlled induction motor drives," in *PESC '90 Rec.*, 1990, pp. 591–598.

[13] E. Levi and V. Vuckovic, "Field-oriented control of induction machines in the presence of magnetic saturation," *Elec. Mach. Power Syst.*, vol. 16, no. 2, pp. 133–147, 1989.

[14] Z. Krzeminski, "Differential equations of induction motor with nonlinear control synthesis with regard to saturation of main magnetic path," *Rozprawy Elektrotechniczne*, vol. 34, no. 1, pp. 117–131, 1988.

[15] W. Leonhard, *Control of Electrical Drives*. New York: Springer-Verlag, 1985, 1990.

[16] J. M. D. Murphy and F. G. Turnbull, *Power Electronic Control of AC Motors*. New York: Pergamon Press, 1988.

[17] G. C. Verghese and S. R. Sanders, "Observers for flux estimation in induction machines," *IEEE Trans. Ind. Electron.*, vol. 35, no. 1, pp. 85–94, Feb. 1988.

[18] R. S. Colby, A. K. Simlot, and M. A. Hallouda, "Simplified model and corrective measures for induction motor instability caused by pwm inverter blanking time," in *PESC '90 Rec. 21st Annu. IEEE Power Electron. Spec. Conf.*, 1990, pp. 678–83.

[19] C. Kao, C. R. Sullivan, B. Acker, and S. R. Sanders, "Induction machine control systems with magnetic saturation," in *PESC '94 Rec. 25st Annu. IEEE Power Electron. Spec. Conf.*, 1994, pp. 250–258.

Charles R. Sullivan (S'92) was born in Princeton, NJ, in 1964. He received the B.S. degree in electrical engineering with highest honors from Princeton University in 1987. He is currently a Ph.D. candidate in electrical engineering at the University of California, Berkeley.

Between 1987 and 1990 he worked at Lutron Electronics, Coopersburg, PA, developing high-frequency dimming ballasts for compact fluorescent lamps. He has published technical papers on numerous topics including thin-film magnetics for high frequency power conversion, dc-dc converter topologies, energy and environmental issues, and modeling, analysis, and control of electric machines.

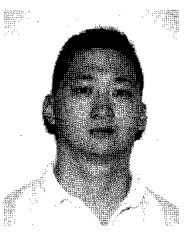

Chaofu Kao was born in Taiwan in 1967. He received the B.S. degree in electrical engineering from the University of Washington in August, 1989. In 1994, he received the M.S. degree in electrical engineering at the University of California, Berkeley.

Between 1989 and 1992, he worked as a sales and application engineer for GE Industrial Power Systems. He presently holds the position of Application Development Manager at GE Fanuc, at joint venture between the General Electric Company and FANUC Ltd. of Japan. At the current time, he is responsible for developing new CNC/motion-control/robotics applications for GE Fanuc.

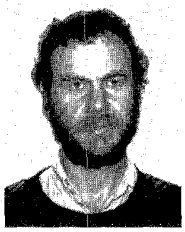

Brian M. Acker received the B.S. degree in electrical engineering with highest honors from the University of California, Berkeley, in 1993. He is currently enrolled in the M.S.E.E. program at Berkeley.

His active research area involves synchronous rectification for dc-dc switching power converters.

Seth R. Sanders (S'88–M'88) received S.B. degrees in electrical engineering and physics from M.I.T., Cambridge, MA, in 1981. He returned to M.I.T. in 1983 and received the S.M. and Ph.D. degrees in electrical engineering in 1985 and 1989, respectively.

From 1981 to 1983, he worked as a design engineer at the Honeywell Test Instruments Division in Denver, CO. He is presently Assistant Professor in the Department of Electrical Engineering and Computer Sciences at the University of California, Berkeley. His research interests are in power electronics, variable speed drive systems, simulation, and in nonlinear circuit and system theory as related to the power electronics field.